Metal Telluride Clusters Composed of Niobocene Carbonyl, Telluride, and Cobalt Carbonyl Units: Syntheses, Structures, and Reactivity

Henri Brunner,[a] Dominique Lucas,[b] Teresa Monzon,[b] Yves Mugnier,[b] Bernhard Nuber,[c] Bernhard Stubenhofer,[a] A. Claudia Stückl,[a] Joachim Wachter,*[a] Robert Wanninger,[a] and Manfred Zabel[a]

Abstract: The reaction of $[Cp^{\#}_2NbTe_2H]$ (**1**$^{\#}$; $Cp^{\#} = Cp^*$ (C_5Me_5) or $Cp^{\times}$ (C_5Me_4Et)) with two equivalents of $[Co_2(CO)_8]$ gives a series of cobalt carbonyl telluride clusters that contain different types of niobocene carbonyl fragments. At 0 °C, $[Cp^{\#}_2NbTe_2Co_3(CO)_7]$ (**2**$^{\#}$) and $[Co_4Te_2(CO)_{10}]$ (**3**) are formed which disappear at higher temperatures: in boiling toluene a mixture of $[cat_2][Co_9Te_6(CO)_8]$ (**5**$^{\#}$) (cat = $[Cp^{\#}_2Nb(CO)_2]^+$) and $[cat_2][Co_{11}Te_7(CO)_{10}]$ (**6**$^{\#}$) is formed along with $[cat][Co(CO)_4]$ (**4**$^{\#}$). Complexes **6**$^{\#}$ transform into $[cat][Co_{11}Te_7(CO)_{10}]$ (**7**$^{\#}$) upon interaction with HPF_6 or wet SiO_2. The molecular structures of **2**($Cp^{\times}$), **4**($Cp^{\times}$), **5**(Cp^*), **6**(Cp^*) and **7**(Cp^*) have been determined by X-ray crystallography. The structure of the neutral **2**($Cp^{\times}$) consists of a $[Co_3(CO)_6Te_2]$ bipyramid which is connected to a $[(C_5Me_4Et)_2Nb(CO)]$ fragment through a μ_4-Te bridge. The ionic structures of **4**($Cp^{\times}$), **5**(Cp^*), **6**(Cp^*) and **7**(Cp^*) each contain one (**4**, **7**) or two (**5**, **6**) $[Cp^{\#}_2Nb(CO)_2]^+$ cations. Apart from **4**, the anionic counterparts each contain an interstitial Co atom and are hexacapped cubic cluster anions $[Co_9Te_6(CO)_8]^{2-}$ (**5**) or heptacapped pentagonal prismatic cluster anions $[Co_{11}Te_7(CO)_{10}]^{n-}$ ($n = 2$: [**6**]$^{2-}$, $n = 1$: [**7**]$^-$), respectively. Electrochemical studies established a reversible electron transfer between the anionic clusters $[Co_{11}Te_7(CO)_{10}]^-$ and $[Co_{11}Te_7(CO)_{10}]^{2-}$ in **6**$^{\#}$ and **7**$^{\#}$ and provided evidence for the existence of species containing $[Co_{11}Te_7(CO)_{10}]$ and $[Co_{11}Te_7(CO)_{10}]^{3-}$. The electronic structures of the new clusters and their relative stabilities are examined by means of DFT calculations.

Keywords: carbonyl complexes · cluster compounds · cobalt · niobium · tellurium

Introduction

Telluride ligands Te_n^{2-} ($n = 1-4$) exhibit a rich coordination chemistry on the boundary between molecular and solid-state chemistry. This is the consequence of their bridging or chelating properties[1] and their ability to form rings or hypervalent centres.[2] Usual reagents are alkali tellurides and polytellurides,[1] trimethylsilyl compounds[3] and organophosphine tellurides.[4] The tellurium transfer, from compounds with labile bonds between a main-group element and Te into inorganic compounds, leads to the formation of aggregates of various size which may be regarded as model compounds for cluster growth.[3] Only a few studies are known that describe the condensation of molecular telluride complexes to give clusters and finally binary solid-state compounds.[4]

The peralkylated niobocene hydrogen ditellurides $[Cp^{\#}_2Nb(Te_2H)]$ (**1**$^{\#}$; $Cp^{\#} = Cp^*$ (C_5Me_5) or $Cp^{\times}$ (C_5Me_4Et)) are novel tellurium transfer reagents that react with $[M(CO)_5THF]$ (M = Cr, W) to give *cyclo*-$[Te_4\{M(CO)_5\}_4]$.[5] In continuation of this work and in order to extend the reactivity potential of **1**$^{\#}$, we now report on its reaction with $[Co_2(CO)_8]$ which gives an insight into the stepwise construction of metal telluride clusters from molecular building blocks. The final products were anionic clusters with different geometries and oxidation states as well as organometallic cationic counterparts. Their electrochemical behaviour as well as their molecular and electronic structures have been investigated.

[a] Dr. J. Wachter, Prof. Dr. H. Brunner, Dr. B. Stubenhofer, Dr. A. C. Stückl, Dipl.-Chem. R. Wanninger, Dr. M. Zabel
Institut für Anorganische Chemie der Universität Regensburg
D-93040 Regensburg (Germany)
Fax: (+49) 941-943-4439
E-mail: joachim.wachter@chemie.uni-regensburg.de

[b] Dr. D. Lucas, T. Monzon, Prof. Y. Mugnier
Laboratoire de Synthèse et d'Electrosynthèse Organométalliques (UMR 5682), Université de Bourgogne
F-21100 Dijon (France)

[c] Dr. B. Nuber
Anorganisch-Chemisches Institut der Universität Heidelberg
D-69120 Heidelberg (Germany)

Results and Discussion

Syntheses, properties and structural characterisation

Reaction at 0 °C: The reaction of $[Co_2(CO)_8]$ with **1**$^{\#}$ was carried out in a 2:1 molar ratio at different temperatures. In THF at 0 °C, the green and violet-brown complexes

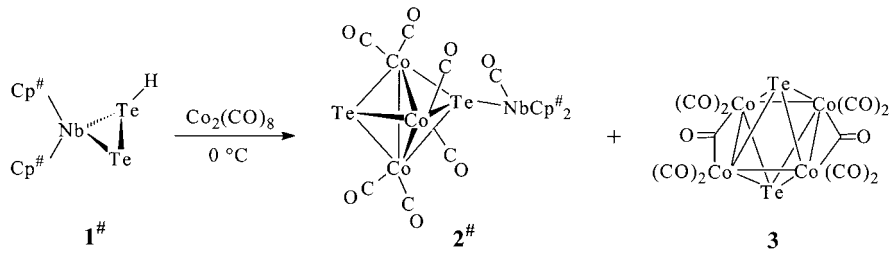

1# 2# 3

Cp# = Cp* (C_5Me_5), Cp× (C_5Me_4Et)

Scheme 1.

$[Cp^{\#}_2NbTe_2Co_3(CO)_7]$ (**2#**) and $[Co_4Te_2(CO)_{10}]$ (**3**) were formed in yields of 5–10% and 70%, respectively (Scheme 1). Both compounds are neutral, diamagnetic and slightly air-sensitive in solution.

The characterisation of the products is based on elemental analyses and X-ray diffraction studies. Field-desorption mass spectroscopy only gave the parent ion for **2#**. The IR spectra (Table 1) of **2#** exhibit, besides absorptions typical of the $Cp^{\#}$ ligands, two bands in the region typical for terminal CO groups. This means that the two expected ν(CO) frequencies of the equivalent $[Co(CO)_2]$ moieties (see below) are superposed by the ν(CO) frequency of the [Nb(CO)] fragment. The ^{1}H NMR spectrum of **2**(Cp*) shows one resonance for the methyl groups on the cyclopentadienyl ring whereas the spectrum of **2**($Cp^{\times}$) contains four such resonances along with two sets of signals for the ethyl groups (Table 2). Attempts to obtain ^{127}Te NMR spectra were not successful.

Table 1. IR data of complexes **2–7**.[a]

	ν(CO) [cm^{-1}]
2(Cp*)	1991 (vs), 1921 (s)
2($Cp^{\times}$)	1995 (vs), 1923 (s)
3	2065 (vs), 2022 (vs), 1997 (vs), 1844 (vs)
	2047 (vs), 2038 (vs), 2018 (vs)[b]
4(Cp*)	2019 (vs), 1960 (vs), 1891 (vs), 1879 (vs)
	2015 (s), 1949 (s), 1887 (vs)[c]
4($Cp^{\times}$)	2022 (vs), 1961 (vs), 1890 (vs), 1879 (vs)
5(Cp*)/**6**(Cp*)	2000 (s), 1945 (vs, br), 1915 (vs)
	2018 (m), 1965 (s), 1930 (vs)[d]
5($Cp^{\times}$)/**6**($Cp^{\times}$)	2010 (s), 1950 (vs, br), 1920 (vs)
	2010 (m), 1960 (s), 1930 (vs)[d]
7(Cp*)	2010 (s), 1945 (vs, br)
	2020 (w), 1965 (s)[d]
7($Cp^{\times}$)	2005 (s), 1940 (vs)

[a] KBr. [b] In toluene. [c] In THF. [d] In CH_2Cl_2.

Table 2. ^{1}H NMR data of complexes **2–7**.[a]

	$\delta(CH_2CH_3)$[b]	δ(Cp-CH_3)	$\delta(CH_2CH_3)$[b]	Solvent
2(Cp*)		1.44 (s, 30H)		C_6D_6
2($Cp^{\times}$)	1.95 (q, 2H)	1.56 (s, 6H)	0.87 (t, 3H)	C_6D_6
	1.83 (q, 2H)	1.51 (s, 6H)	0.80 (t, 3H)	
		1.45 (s, 6H)		
		1.42 (s, 6H)		
4(Cp*)		1.95 (s, 30H)		CD_2Cl_2
4($Cp^{\times}$)	2.23 (q, 4H)	1.98 (s, 24H)	1.13 (t, 6H)	CD_2Cl_2
5(Cp*)/**6**(Cp*)		1.97 (s, 30H)		CD_2Cl_2
5($Cp^{\times}$)/**6**($Cp^{\times}$)	2.21 (q, 4H)	1.96 (s, 24H)	1.13 (t, 6H)	CD_2Cl_2
7(Cp*)		2.06 (s, 30H)		[D_6]acetone
		1.98 (s, 30H)		CD_2Cl_2
7($Cp^{\times}$)	2.38 (q, 4H)	2.09 (s, 12H)	1.12 (t, 6H)	[D_6]acetone
		2.06 (s, 12H)		
	2.22 (q, 4H)	1.96 (s, 12H)	1.18 (t, 6H)	CD_2Cl_2
		1.95 (s, 12H)		

[a] Bruker WM250 spectrometer, TMS, 250 MHz, 24 °C. [b] ^3J(CH,H) = 6.6–7.4 Hz.

An X-ray diffraction analysis of a single crystal of **2**($Cp^{\times}$) grown in toluene/pentane (1:2) reveals that the molecule consists of a trigonal-bipyramidal cobalt telluride cluster to which a niobocene carbonyl fragment is coordinated at one of the apical tellurides (Figure 1, Table 3; a comparison of bond

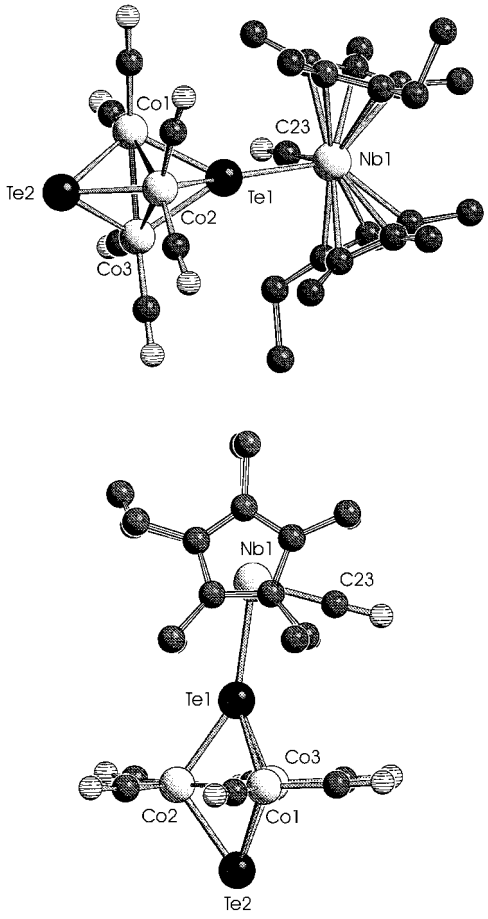

Figure 1. The molecular structure of **2**($Cp^{\times}$) in two views (Schakal plot).

lengths with complexes **3–5** and **7** is also given in Table 4 later). A nearly equilateral Co_3 triangle is capped by two Te bridges, while each Co atom bears two CO groups to give rise to 47 cluster valence electrons. The attached $[Cp^{\times}_2Nb(CO)]$ fragment serves as a one-electron donor, which thus provides a closed valence shell for the whole cluster. The C23-Nb-Te1 angle is slightly smaller (82.8(3)°) than related angles in other

0947-6539/00/0603-0494 $ 17.50+.50/0 *Chem. Eur. J.* **2000**, *6*, No. 3

Table 3. Selected bond lengths [Å] and angles [°] for $[(C_5Me_4Et)_2NbCo_3(CO)_7Te_2]$ **2**($Cp^{\times}$).

Nb1–C23	2.023(11)	Te2–Co2	2.480(2)
Nb1–Te1	2.836(2)	Te2–Co3	2.489(2)
Te1–Co1	2.482(2)	Co1–Co2	2.520(3)
Te1–Co2	2.466(2)	Co1–Co3	2.505(3)
Te1–Co3	2.487(2)	Co2–Co3	2.513(3)
Te2–Co1	2.485(2)		
Te1-Nb1-C23	82.8(3)	Te1-Co2-Te2	109.0(1)
Nb1-Te1-Co1	137.7(1)	Te1-Co3-Te2	108.0(1)
Nb1-Te1-Co2	152.2(1)	Te1-Co1-Co2	59.1(1)
Nb1-Te1-Co3	141.3(1)	Te1-Co1-Co3	59.8(1)
Co1-Te1-Co2	61.2(1)	Te1-Co2-Co1	59.7(1)
Co1-Te1-Co3	60.5(1)	Te1-Co2-Co3	59.9(1)
Co1-Te2-Co2	61.0(1)	Te1-Co3-Co1	59.6(1)
Co1-Te2-Co3	60.5(1)	Te1-Co3-Co2	59.1(1)
Co1-Co2-Co3	59.7(1)	Te2-Co1-Co2	59.4(1)
Co1-Co3-Co2	60.3(1)	Te2-Co1-Co3	59.8(1)
Co2-Te1-Co3	61.0(1)	Te2-Co2-Co1	59.6(1)
Co2-Te2-Co3	60.8(1)	Te2-Co2-Co3	59.8(1)
Co2-Co1-Co3	60.0(1)	Te2-Co3-Co1	59.7(1)
Te1-Co1-Te2	108.3(1)	Te2-Co3-Co2	59.5(1)

niobocene(III) derivatives, for example $[(C_5H_5)_2Nb(CO)SR]$ complexes with angles between 88.5[6] and 92.3°.[7]

The IR spectrum of complex **3** (Table 1) in KBr exhibits three terminal CO absorptions and one absorption in the bridging region, whereas in solution there are only three terminal CO bands. A single-crystal structure determination revealed the composition $[Co_4(CO)_{10}Te_2]$. The tetragonal-bipyramidal structure in which a Co_4 rectangle is bridged by two Te atoms has been reported previously.[8] Each Co atom bears two terminal CO groups; the remaining two CO groups bridge opposite sides of the Co rectangle. Complex **3** belongs to the family of $[Co_4(CO)_{10}E_2]$ (E = S, Te, PPh, AsPh) complexes.[8, 9]

Reaction products at higher temperatures: At room temperature **2**# and **3** are formed in negligible quantities; the major products are ionic compounds, the formation of which is completed by refluxing the mixture in toluene for 3 h [Eq. (1)]. During this procedure a dark precipitate formed

$$[Cp^{\#}_2NbTe_2H] + [Co_2(CO)_8] \xrightarrow[110\,^{\circ}C]{\text{toluene}} [cat][Co(CO)_4]\ (\mathbf{4^{\#}}) + [cat_2][Co_9Te_6(CO)_8]\ (\mathbf{5^{\#}}) + [cat_2][Co_{11}Te_7(CO)_{10}]\ (\mathbf{6^{\#}}) \quad (1)$$

$cat = [Cp^{\#}_2Nb(CO)_2]^+$

and the liquid phase became pale yellow. From this solution the yellow compounds **4**# were isolated in 6–19% yield after chromatography on Sephadex. Characterisation of **4**# and the dark material (see below) is based on elemental analyses and X-ray diffraction studies. Positive- and negative-field desorption mass spectroscopy gave, in all cases, only mass peaks corresponding to the $[Cp^{\#}_2Nb(CO)_2]^+$ cations.

The IR spectra of **4**# in KBr show four strong absorptions of equal intensity (Table 1). From information obtained from an X-ray diffraction study (see below), they may be attributed to the absorption patterns of terminal CO groups of the $[Cp^{\#}_2Nb(CO)_2]^+$ (C_{2v} symmetry) and $[Co(CO)_4]^-$ (T_d symmetry) ions; the latter gives rise to one band at 1897 cm^{-1} in THF. The ^1H NMR spectra exhibit a singlet for the ring methyl groups of **4**(Cp*) and a singlet, a quartet and a triplet typical of the C_5Me_4Et ligand of **4**($Cp^{\times}$) (Table 2). The crystal structure of **4**($Cp^{\times}$) consists of ion pairs of distinct $[Cp^{\times}_2Nb(CO)_2]^+$ and $[Co(CO)_4]^-$ ions (Figure 2). The latter exhibits Co–C bond lengths between 1.719(8) and 1.767(8) Å (Table 4); the C-Co-C angles (106.7(4)–111.8(4)°) do not

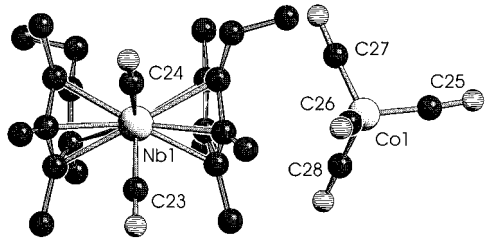

Figure 2. Molecular unit of the crystal structure of $[Cp^{\times}_2Nb(CO)_2][Co(CO)_4]$ (**4**($Cp^{\times}$); Schakal plot).

significantly deviate from tetrahedral geometry. It is striking that one face of the $[Co(CO)_4]$ tetrahedron lies directly over one of the $Cp^{\times}$ ring planes. The corresponding C–H···O contacts are about 2.9 Å, which suggests a further example of hydrogen-bonding acceptor CO ligands.[10] The skeleton of the niobocene-derived cation is related to that in $[Cp^{\times}_2NbCl_2]$[11] and $[Cp^{\times}_2NbF_2]PF_6$.[11] The mean Nb–CO bond lengths are 2.057(7) Å, the OC-Nb-CO angle is 86.6(3)°. Angles in the same range have been found in the related compounds $[Cp^{*}_2M(CO)_2]$ (M = Ti, Zr, Hf)[12] and $[(C_5H_5)_2V(CO)_2][Co(CO)_4]$.[13]

Table 4. Comparison of important distances [Å] of compounds **2**–**7**.

	2($Cp^{\times}$)	**3**[8]	**4**($Cp^{\times}$)	**5**(Cp*)	**7**(Cp*)
μ_3-Te–Co	2.485(3)				
μ_4-Te–Co	2.478(2)	2.544(2)		2.500(2)–2.528(2)	2.498(3)–2.523(3)
μ_5-Te–Co					2.552(3)–2.581(3)
Te–Co_{bc}[a]				2.945(1)–2.975(1)	2.631(3), 2.649(3)
Te–Nb	2.836(2)				
Te···Te	4.007	3.306			
Co–Co	2.513(3)	2.589(2)–2.873(2)		2.763(2)–2.772(2)	2.522(4)–2.612(4)
Co–Co_{bc}[a]				2.397(2)–2.401(2)	2.522(4)–2.544(3)
Co–C_{ter}[b]		1.79(2)	1.74(1)	1.746(9)	1.75(2)
Co–C_{br}[b]		1.93(1)			
Nb–CO[b]	2.023(11)		2.056(7)	2.061(8)	2.04(2)

[a] Body-centered Co. [b] Average values.

Recrystallisation of the dark precipitate described above from acetonitrile gave dark crystals with differing morphology. Under the microscope it was possible to distinguish prisms and needles and to separate some of them for X-ray crystallography. As a consequence, the shiny black prisms were found to be compound **5**(Cp*) and the dark needles were compound **6**(Cp*). The elemental analyses did not allow a clear assignment to one of the two compounds. In the case of the C_5Me_5 ligand, values of C and H were scattered in an unsystematic manner between those for **5**(Cp*) and **6**(Cp*) and for the C_5Me_4Et ligand the C and H values were always close to those of **6**(Cp$^{\times}$) (see Experimental Section, Table 8).

The crystal structure of **5**(Cp*) consists of four molecular units in the monoclinic cell and each molecular unit contains two $[Cp^*_2Nb(CO)_2]^+$ cations and one $[Co_9Te_6(CO)_8]^{2-}$ anion (Tables 4, 5). The geometry of the niobocene moiety is analogous to that found in **4**(Cp$^{\times}$); its charge of +1 follows from the sharp ^{1}H NMR resonances and the absence of any ESR signal for the mixture of **5** and **6** (Table 2), which indicates the presence of Nb^{III}. The cluster anion of **5**(Cp*) can be described as a hexacapped Co_8 cube with an interstitial Co atom (Figure 3); a crystallographic C_2 axis passes through Te2, Co1 and Te4. Formally, if each Te ligand is considered to be Te^{2-}, then there are eight Co^{I} and one Co^{II} centres. The remaining two negative charges are compensated by the cations. An alternative view is that of an "anti-chevrel cluster"[14] in which the central Co atom is surrounded by a cube of eight Co atoms and an octahedron of six Te atoms. The inner Co–Co bond lengths, Co1–Co2 for example, are remarkably short (average 2.40 Å), whereas the outer Co–Co bond lengths, Co2–Co3 for example, are much longer (average 2.77 Å). For comparison, Co–Co bond lengths in $[Co_8S_6(SPh)_8]^{4-}$, in which the Co atoms form an empty cube, are on average 2.66 Å.[15] The Te–Co bond lengths also exhibit two different ranges, namely 2.528(2) Å for Te1–Co2 compared with 2.975(2) Å for Te1–Co1.

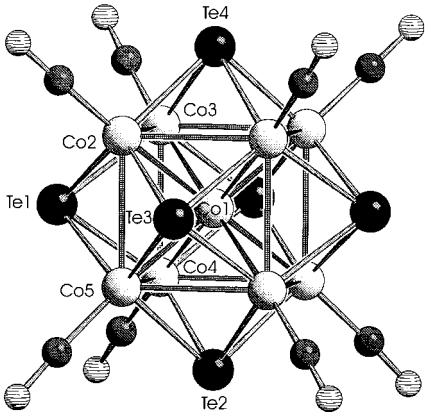

Figure 3. Schakal plot of the $[Co_9Te_6(CO)_8]^{2-}$ anion of **5**(Cp*).

Table 5. Selected bond lengths [Å] and angles [°] for $[(C_5Me_5)_2NbCO)_2]_2$-$[Co_9Te_6(CO)_8]$ **5**(Cp*).

Te1–Co1	2.975(2)	Te4–Co3	2.501(2)
Te1–Co2′	2.528(2)	Te4–Co3′	2.501(2)
Te1–Co3	2.514(2)	Co1–Co2	2.401(2)
Te1–Co4	2.516(2)	Co1–Co3	2.397(2)
Te1–Co5	2.528(2)	Co1–Co4	2.401(2)
Te2–Co1	2.951(2)	Co1–Co5	2.391(2)
Te2–Co4	2.508(2)	Co2–Co3	2.773(2)
Te2–Co4′	2.509(2)	Co2–Co3′	2.769(2)
Te2–Co5	2.501(2)	Co2–Co5′	2.767(2)
Te2–Co5′	2.501(2)	Co3–Co4	2.773(1)
Te3–Co1	2.968(1)	Co4–Co5	2.764(2)
Te3–Co2	2.522(2)	Co4–Co5′	2.766(2)
Te3–Co3	2.515(2)	Co5–Te3′	2.528(2)
Te3–Co4	2.511(2)	Co5–Co2′	2.766(2)
Te3–Co5′	2.528(2)	Co5–Co4′	2.766(2)
Te4–Co1	2.945(2)	Co–C_{mean}	1.745(9)
Te4–Co2	2.510(2)	Nb1–C11	2.055(8)
Te4–Co2′	2.510(2)	Nb2–C31	2.058(7)
Co3-Te1-Co1	50.94(3)	Co5′-Co1-Co5	109.23(7)
Co3-Te1-Co2′	66.61(3)	Co5′-Co1-Co2′	179.74(6)
Co3-Te1-Co4	66.89(3)	Co5-Co1-Co2′	70.52(3)
Co3-Te1-Co5	101.65(3)	Te4-Co1-Te2	180.00(5)
Co4-Te1-Co2′	101.98(3)	Te3-Co1-Te3′	180.00(5)
Co4-Te1-Co5	66.44(3)	Co1-Co2-Te4	73.68(4)
Co5-Te1-Co2′	66.31(3)	Te4-Co2-Te3	112.38(4)
Co5-Te2-Co5′	102.45(5)	Co1-Co2-Co5′	54.59(4)
Co5-Te2-Co4	66.98(3)	Te4-Co2-Co5′	128.27(5)
Co5-Te2-Co1	51.22(2)	Co5′-Co2-Co3′	89.87(4)
Co4-Te3-Co3	66.96(3)	Co5′-Co2-Co3	89.96(4)
Co4-Te3-Co2	102.23(3)	Co3′-Co2-Co3	89.79(4)
Co4-Te3-Co1	51.15(3)	Te4-Co3-Te1	113.22(4)
Co3′-Te4-Co3	102.88(4)	C11′-Nb1-C11	85.7(4)
Co3′-Te4-Co2′	67.19(4)	C31′-Nb2-C31	89.7(3)
Co3′-Te4-Co1	51.44(2)		

The $[Co_9Te_6(CO)_8]^{2-}$ anion belongs to the family of metal-centered hexacapped $[M_9(\mu_4\text{-}E)_6L_8]$ clusters (M = Ni, Pd; E = GeEt, As, Te).[14, 16] There are 123 metal valence electrons (MVE) $[(9\times9)+(8\times2)+(6\times4)+2]$, which lies in the range of 120–130 MVE already reported for this type of cluster.[17] The only compound with a somewhat related Co_9 array is the tetracapped cluster anion $[Co_9Bi_4(CO)_{16}]^{2-}$, in which the cobalt atoms are significantly tetragonally distorted.[18]

The structure determination of **6**(Cp*) was handicapped by symmetry problems. From the systematic absences, the space group *Pnma* was derived for the starting calculations. The cluster anion $[Co_{11}Te_7(CO)_{10}]$ and two Nb atoms could be located by direct methods and refined unambiguously. However, it was not possible to find all the C atoms associated with the Nb cations. Evidently, the assumed space group symmetry is not yet correct and must be regarded as pseudosymmetry, generated by the fairly high symmetry of the cluster anion. On account of these results, one $[Co_{11}Te_7(CO)_{10}]^{2-}$ and two $[Cp^*_2Nb(CO)_2]^+$ ions may be present. In the structure of **7**(Cp*), which is an oxidation product of **6**(Cp*) (see below), both ionic species exist in a 1:1 ratio. Elemental analyses of **6**$^{\#}$ (Table 8 in the Experimental Section) are in agreement with a 2:1 ratio of cations to anions, regardless of contamination with **5**$^{\#}$, since the C and H values of the latter are within the same range.

Transformations of the cobalt telluride clusters: Column chromatography on silica gel (activity II/III) of the **5**$^{\#}$/**6**$^{\#}$ precipitates obtained from the reaction at 110 °C gave complexes **7**$^{\#}$ in yields between 42 and 64 % with respect to **1**$^{\#}$ [Eqs. (1) and (2)]. Elemental analyses (Table 8 in the

$$[cat_2][Co_{11}Te_7(CO)_{10}]\ (\mathbf{6}^{\#}) \xrightarrow{H^+} [cat][Co_{11}Te_7(CO)_{10}]\ (\mathbf{7}^{\#}) \quad (2)$$

0947-6539/00/0603-0496 $ 17.50+.50/0 *Chem. Eur. J.* **2000**, *6*, No. 3

Experimental Section) are significantly poorer in C and H; this indicates a transformation of **6**# into **7**# by loss of one $[Cp^{\#}_2Nb(CO)_2]^+$ unit. Additionally, there is no hint of the presence of complexes **5**#. The transformation can be monitored by IR spectroscopy (Table 1). Whereas the mixture of, for example, **5**(Cp*) and **6**(Cp*) contains three CO absorptions at 2000, 1945 and 1915 cm^{-1}, **7**(Cp*) shows only two bands at 2010 and 1945 cm^{-1}. Thus, it is likely that the ν(CO) frequency at 1915 cm^{-1} belongs to **6**(Cp*); this is also supported by electrochemical experiments (see below). One of the two CO absorptions expected for the $[Cp^{*}_2Nb(CO)_2]^+$ fragment in **7**(Cp*) is superposed by the very strong and broad absorption of the equivalent terminal CO groups of the cluster anion.

The transformation of **6**(Cp*) into **7**(Cp*) has also been observed when the original mixture of **5**(Cp*) and **6**(Cp*) was stirred with HPF_6 [Eq. (2)]. One may assume H_2 to be a further reaction product that only forms in very low quantities. After washing with H_2O and recrystallisation from CH_2Cl_2, pure **7**(Cp*) was obtained. The fate of **5**(Cp*) is still unknown. The transformation did not occur on basic Al_2O_3.

The crystal structure of **7**(Cp*) consists of two molecular units in the monoclinic cell and each molecular unit contains one pair of $[Cp^{*}_2Nb(CO)_2]^+$ and $[Co_{11}Te_7(CO)_{10}]^-$ ions. The geometry of the niobocene cation is analogous to that found in **4**($Cp^{\times}$) and **6**(Cp*). The cluster anion is best described by a pentagonal prism formed by ten Co atoms in the centre of which resides a further Co atom (Figure 4, Table 6). The faces

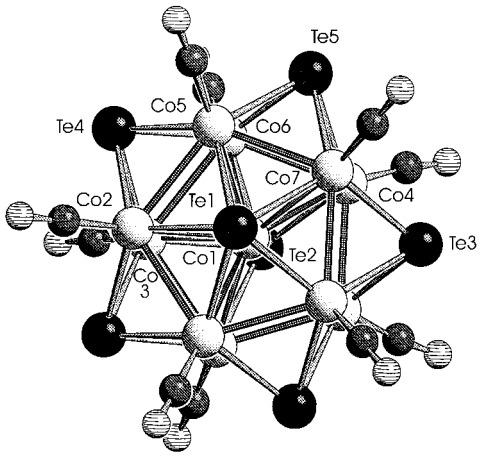

Figure 4. Schakal plot of the $[Co_{11}Te_7(CO)_{10}]^-$ anion of **7**(Cp*).

of the prism are capped by two μ_5- and five μ_4-Te^{2-} ligands. In contrast to the cubic anion in **5**(Cp*), all Co–Te and Co–Co bond lengths are approximately of equal order (Tables 4, 6) so that nearly perfect edge-sharing octahedra are arranged around the fivefold Te1-Co1-Te2 axis, with the centered Co1 atom as the common vertex. A similar structure has been found for $[Ph_4P]_2[Co_{11}Te_7(CO)_{10}]$, which was synthesised from $[Co_2(CO)_8]$ and Na_2Te_2 in a 3:2 ratio and Ph_4PCl under solvothermal conditions.[19] In this cluster salt, it is evident that the anion bears a twofold negative charge to give a metal valence electron count of 149 MVE $[(11\times 9)+(10\times 2)+(7\times 4)+2]$. However, the presence of a dianion in **7**# would

Table 6. Selected bond lengths [Å] and angles [°] for $[(C_5Me_5)_2NbCO)_2][Co_{11}Te_7(CO)_{10}]$ **7**(Cp*).

Te1–Co1	2.631(3)	Co1–Co2	2.563(4)
Te1–Co2	2.577(3)	Co1–Co3	2.572(4)
Te1–Co5	2.581(2)	Co1–Co4	2.549(3)
Te1–Co7	2.565(3)	Co1–Co5	2.544(3)
Te2–Co1	2.649(3)	Co1–Co6	2.567(3)
Te2–Co3	2.581(3)	Co1–Co7	2.556(3)
Te2–Co4	2.570(2)	Co2–Co3	2.612(4)
Te2–Co6	2.552(2)	Co2–Co5	2.592(3)
Te3–Co4	2.523(2)	Co3–Co6	2.577(3)
Te3–Co7	2.500(3)	Co4–Co6	2.611(3)
Te4–Co2	2.510(2)	Co4–Co7	2.616(3)
Te4–Co3	2.510(2)	Co4–Co4A	2.522(4)
Te4–Co5	2.498(2)	Co5–Co6	2.617(3)
Te4–Co6	2.515(2)	Co5–Co7	2.574(3)
Te5–Co4	2.499(2)	Co7–Co7A	2.600(4)
Te5–Co5	2.519(2)	Co_{2-7}–C_{14-19}	1.71–1.77(3)
Te5–Co6	2.510(2)	Nb1–C_{Cp}	2.37–2.42(3)
Te5–Co7	2.517(2)	Nb1–C13	2.042(15)
Co1-Te1-Co2	59.0(1)	Te1-Co1-Co2	59.5(1)
Co2-Te1-Co7	109.0(1)	Te2-Co1-Co2	120.4(1)
Co1-Te2-Co3	58.9(1)	Co2-Co1-Co4	149.9(1)
Co3-Te2-Co4	109.1(1)	Co3-Co1-Co4	110.0(1)
Co4-Te3-Co7	62.8(1)	Te1-Co2-Te4	118.5(1)
Co7-Te3-Co4A	93.6(1)	Te1-Co2-Co3	121.2(1)
Co2-Te4-Co3	62.7(1)	Te4-Co2-Co3	58.7(1)
Co3-Te4-Co5	94.1(1)	Co3-Co2-Co5	89.6(1)
Co4-Te5-Co5	94.0(1)	Co5-Co2-Co5A	107.6(1)
Co4-Te5-Co6	62.8(1)	C13-Nb1-C13A	85.3(9)
Te1-Co1-Te2	180.0(3)	Nb1-C13-O13	177.1(14)

imply a paramagnetic Nb^{IV} centre in a d^1 configuration in the counterion; this is not in agreement with the sharp resonances of the Cp# ligands of **7**# in the ^1H NMR spectra. Furthermore, the chemical shifts observed for **7**# are identical with those observed for **4**# and the **5**#/**6**# mixtures in which the niobocene units are definitively diamagnetic. Also, samples of **7**# are ESR silent. On account of these considerations, we conclude the cluster anion in **7**# to have 148 MVE, which is strongly supported by electrochemistry and density functional calculations (see below).

Electrochemical investigations: Above we postulated the transformation of the cluster anion $[Co_{11}Te_7(CO)_{10}]^{2-}$ into $[Co_{11}Te_7(CO)_{10}]^-$ by the interaction of **6**# with H^+ [Eq. (2)]. Therefore, the electron-transfer properties of **6**(Cp*) and **7**($Cp^{\times}$) were examined by electrochemical methods. In THF (Bu_4NPF_6 as the supporting electrolyte), the polarogram of **7**(Cp*) showed one oxidation wave E′ ($E_{1/2}=+0.35$ V) and four reduction waves A, B, C and D ($E_{1/2}=-0.32$, -1.04, -1.55, and -1.88 V, respectively). The heights of waves E′, A and B were nearly equal, whereas wave C was twice as high as B (Figure 5a). In cyclic voltammetry, two one-electron reversible systems A/A′ and B/B′ appeared in the potential range between 0 and -1.3 V. For these two processes the peak currents increased linearly with $V^{1/2}$ and the half-wave potentials were independent of the scan rate. The peak shapes were characterised by $|E_{pc}-E_{pa}|\approx 65$ mV at scan rates up to 0.2 $V s^{-1}$. The values are in agreement with the theoretical values for diffusion-controlled one-electron transfer and this was verified by controlled potential electrolysis at -0.6 V, which gave 1.0 ± 0.1 e for the first reduction step. The

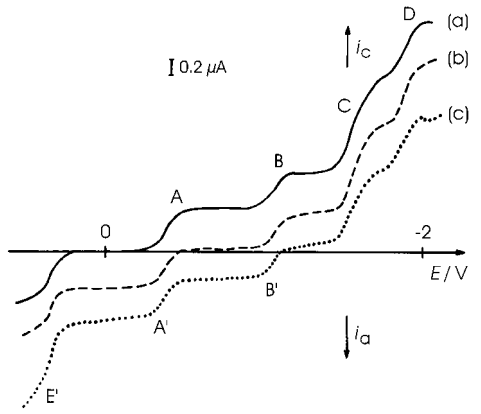

Figure 5. Polarograms (average current) of **7**(Cp*) in THF (0.2 M Bu_4NPF_6 solution): a) initial polarogram; b) after one-electron reduction at -0.6 V; c) after reduction at -1.2 V.

polarogram of the resulting solution exhibited the two oxidation waves E′ and A′ and the reduction waves B, C, and D (Figure 5b). IR spectroscopy showed that the initial strong absorption band at 1961 cm^{-1}, ascribed to ν(CO) of $[Co_{11}Te_7(CO)_{10}]^-$ (Table 1), had disappeared and an absorption at 1926 cm^{-1}, belonging to $[Co_{11}Te_7(CO)_{10}]^{2-}$, had appeared (Figure 6). The solution was ESR silent.

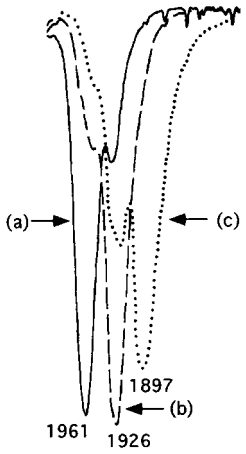

Figure 6. IR spectra [cm^{-1}] in THF of **7**(Cp*) a) before electrolysis; b) after one-electron reduction at -0.6 V; c) after reduction at -1.2 V.

Further electrolysis at -1.2 V (plateau of wave B) consumed between 1.3 e (low temperature) and 1.8 e (room temperature). In polarography three oxidation waves E′, A′ and B′ and two reduction waves C and D were observed (Figure 5c). The electrolysed solution exhibited a new absorption at 1897 cm^{-1} in the IR spectrum (Figure 6) which may be ascribed to the still elusive $[Co_{11}Te_7(CO)_{10}]^{3-}$ anion. However, this solution was unstable and transformed into a solution that exhibited a ten-line signal in the ESR spectrum ($g = 1.9971$, $a_{Nb} = 29.69$ G), which may be attributed to a Nb^{II} species ($I = 9/2$),[11] probably the still unknown 19 e complex $[Cp^*_2Nb(CO)_2]$. Concommittantly, the CO absorption at 1926 cm^{-1} ($[Co_{11}Te_7(CO)_{10}]^{2-}$) reappeared (Figure 6) and reduction wave B appeared, while the oxidation wave B′ decreased. A possible explanation for the latter process would be an electron transfer between the cluster anion and the niobocene cation [Eq. (3)].

$$[Co_{11}Te_7(CO)_{10}]^{3-} + [Cp^{\#}_2Nb(CO)_2]^+ \rightleftharpoons [Co_{11}Te_7(CO)_{10}]^{2-} + [Cp^{\#}_2Nb(CO)_2] \quad (3)$$

Wave E′ may be attributed to the oxidation of $[Co_{11}Te_7(CO)_{10}]^-$. In order to avoid polymerisation of THF, the oxidative electrolysis of **7**(Cp*) was performed in CH_2Cl_2/Bu_4NPF_6 solution. After oxidation at $E = +0.5$ V, the reduction wave E was observed at the same potential as that of wave E′. The solution was ESR silent, which thus excludes the participation of a Nb^{IV} species.

The processes concerning waves C and D are mainly related with the cationic part of **7**(Cp*), as has been verified by separate investigations of $[Cp^*_2Nb(CO)_2][Co(CO)_4]$ (**4**(Cp*); see below). However, it must be stressed that wave C is twice as high as waves A and B when compared with the corresponding reduction of **4**(Cp*). This indicates the participation of the cluster anion as discussed in the preceding paragraphs.

Analogous observations have been made for solutions of the **5**(Cp*)/**6**(Cp*) mixture: after oxidation at $E = 0$ V, the initial IR absorption at 1926 cm^{-1} ($[Co_{11}Te_7(CO)_{10}]^{2-}$) transformed into that at 1961 cm^{-1} ($[Co_{11}Te_7(CO)_{10}]^-$). Reduction of $[Co_{11}Te_7(CO)_{10}]^{2-}$, evolution of $[Co_{11}Te_7(CO)_{10}]^{3-}$ into $[Co_{11}Te_7(CO)_{10}]^{2-}$ and formation of a paramagnetic species were also observed.

The electrochemical behaviour of **4**(Cp*) was studied as a reference sample for the redox active Nb^{III} centre.[11, 20] Polarography of **4**(Cp*) gave one oxidation wave F′ at $E = -0.26$ V and two reduction waves C and D at -1.54 and -1.88 V, respectively. The height of the three waves was nearly equal. Cyclic voltammetry of **4**(Cp*) gave an irreversible system F/F_1' ($\Delta E_p = 280$ mV) in the anodic potential sweep because of the formation of $[Co_2(CO)_8]$.[21] Two reversible systems C/C′ and D/D′ were found in the cathodic potential range (Figure 7) at potentials comparable with waves C/C′ and D/D′ observed for the cluster anion $[Co_{11}Te_7(CO)_{10}]^-$ (Figure 5). Additionally, the same ten-line ESR system was

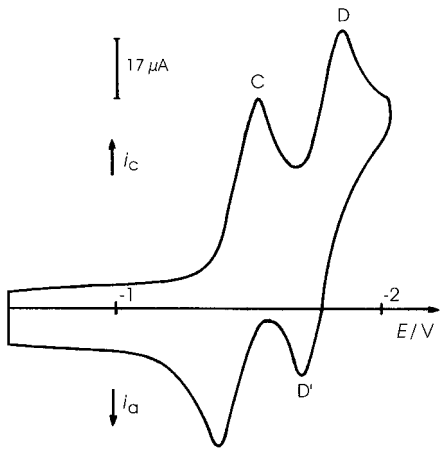

Figure 7. Cyclic voltammogram of $[Cp^*_2Nb(CO)_2][Co(CO)_4]$ in THF (0.2 M Bu_4NPF_6 solution) on a vitreous carbon electrode. Initial potential: -0.6 V, sweep rate 0.02 $V s^{-1}$.

0947-6539/00/0603-0498 $ 17.50+.50/0 *Chem. Eur. J.* **2000**, *6*, No. 3

found for the first electrogenerated species as described above, and which was tentatively attributed to $[Cp^*_2Nb(CO)_2]$. The nature of the second species is still speculative.

In summary, the electrochemical results show that the anionic clusters $[Co_{11}Te_7(CO)_{10}]^{n-}$ are the redox-active components of **6#** and **7#**. They also show that there are additional electron-transfer processes that lead to species $[Co_{11}Te_7(CO)_{10}]$ and $[Co_{11}Te_7(CO)_{10}]^{3-}$ [Eq. (4)].

$$[Co_{11}Te_7(CO)_{10}] \underset{E/E'}{\overset{+0.33\,V}{\rightleftharpoons}} [Co_{11}Te_7(CO)_{10}]^- ([\mathbf{7}]^-) \underset{A/A'}{\overset{-0.32\,V}{\rightleftharpoons}} [Co_{11}Te_7(CO)_{10}]^{2-} ([\mathbf{6}]^-) \underset{B/B'}{\overset{-1.04\,V}{\rightleftharpoons}} [Co_{11}Te_7(CO)_{10}]^{3-} \quad (4)$$

DFT calculations: The relatively rare pentagonal-prismatic geometry and the unexpected electron-transfer capacity of the prepared cluster anions led us to investigate the electronic structures within the $[Co_{11}Te_7(CO)_{10}]^{n-}$ $(n=0-3)$ series by means of DFT methods and to calculate the cubic $[Co_9Te_6(CO)_8]^{n-}$ clusters $(n=0,\ 2)$ for comparison. The resulting bonding energies and molecular orbital compositions as well as the results from hardness and charge partitioning analysis are discussed in terms of stability prediction and redox activities of the compounds.

From the bonding energy calculations, $[Co_{11}Te_7(CO)_{10}]^{n-}$ generally will be formed with a higher probability than $[Co_9Te_6(CO)_8]^{n-}$ (Figure 8). The minimum of the $E_{bonding}$ function versus cluster charge is a hypothetic state with the

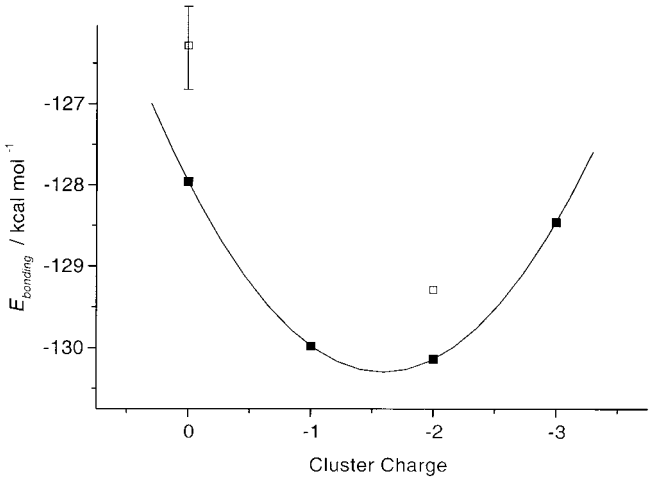

Figure 8. Average bonding energy per atom as a function of the negative cluster charge n: $E_{bonding}=f(n)$ with $n=0-3$; ■ = $[Co_{11}Te_7(CO)_{10}]^{n-}$; □ = $[Co_9Te_6(CO)_8]^{n-}$. The amount of energy contributed by one μ_4-Te is indicated for $[Co_9Te_6(CO)_8]^0$.

fractional charge of $-1.6\,e^-$. Hence it can be seen that $[Co_{11}Te_7(CO)_{10}]^-$ and $[Co_{11}Te_7(CO)_{10}]^{2-}$ almost share the position of the most stable cluster within the series. The cubic cluster may occur with charge of -2 if the reaction conditions do not support the formation of highly charged $[Co_{11}Te_7(CO)_{10}]^{3-}$ ion. Formally, the pentagonal prism is obtained from the cube by adding one $[Co_2(CO)_2Te]$ unit. The mean bonding energy increases during this step by ≈ 1 kcal mol^{-1} per atom as a result of the stabilising effects of additional Co–Co interactions. The contribution of one μ_4-Te atom was hereby estimated to be only ≈ 0.5 kcal mol^{-1} (see the "error bar" in Figure 8).

The frontier orbitals have been calculated and are depicted for the examples $[Co_{11}Te_7(CO)_{10}]^-$ and $[Co_9Te_6(CO)_8]^{2-}$ in Figure 9. For the polyhedra with D_{4h} and D_{5h} symmetry,

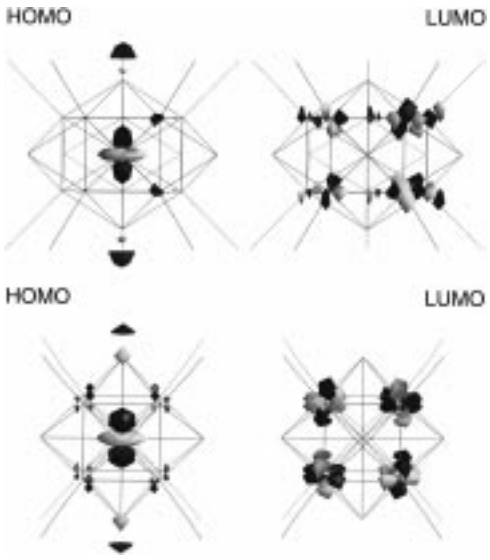

Figure 9. HOMO and LUMO electron-density distribution of $[Co_{11}Te_7(CO)_{10}]^-$ (top) and $[Co_9Te_6(CO)_8]^{2-}$ (bottom). The high-density iso-surface is plotted.

several linear combinations of Co d states are found to describe the main part of the interactions between the cage Co atoms (type Co2). The central Co1 atoms mainly contribute to the HOMOs. Influenced by the p and s orbitals of the apical Te atoms and by the geometry of the cage, the d_{z^2} orbital forms the doubly occupied a_1' state of $[Co_{11}Te_7(CO)_{10}]^-$ as well as the singly occupied a_{1g} state of $[Co_9Te_6(CO)_8]^{2-}$. The depicted LUMOs are, for example, antibonding Co d linear combinations (e_2'' in $[Co_{11}Te_7(CO)_{10}]^-$, e_g in $[Co_9Te_6(CO)_8]^{2-}$). The same type of HOMO and LUMO is found for $[Co_{11}Te_7(CO)_{10}]$. The e_2'' state of the pentagonal prisms is singly occupied in $[Co_{11}Te_7(CO)_{10}]^{2-}$ and doubly in $[Co_{11}Te_7(CO)_{10}]^{3-}$. Because the Co2 d_{zx}/d_{yz} linear combinations are of antibonding nature here, bonding within the cage will be weakened by the occupation of this state. On the other hand, the additional electrons are distributed almost equally among the ten participating Co atoms and their interactions are close to metallic. So, even the highly charged species $[Co_{11}Te_7(CO)_{10}]^{3-}$ could be realised.

As for related compounds,[17, 22, 23] the calculated gap-energies within the $[Co_{11}Te_7(CO)_{10}]^{n-}$ series are relatively small. This underlines the metal-like character of the studied cluster species and explains the dark colour of the compounds. Particularly $[Co_{11}Te_7(CO)_{10}]^-$ shows a HOMO–LUMO gap of only 0.088 eV and is therefore very sensitive to electron transfer. $[Co_{11}Te_7(CO)_{10}]$ (0.171 eV), $[Co_{11}Te_7(CO)_{10}]^{2-}$ (0.582 eV) and $[Co_{11}Te_7(CO)_{10}]^{3-}$ (0.559 eV) are more stable in that respect, whereas $[Co_9Te_6(CO)_8]^{2-}$ has the largest gap (nearly 1 eV).

The orbital picture reveals further stabilising effects. In the case of a singly occupied degenerated state e''_2 in $[Co_{11}Te_7(CO)_{10}]^{2-}$, the distortion of the geometry by symmetry breaking according to the Jahn–Teller theorem might occur. This would result in an additional energy gain. Therefore, in its distorted form, $[Co_{11}Te_7(CO)_{10}]^{2-}$ would be a good candidate for a stable ground state within the $[Co_{11}Te_7(CO)_{10}]^{n-}$ series. In $[Co_9Te_6(CO)_8]$ as well as in $[Co_9Te_6(CO)_8]^{2-}$, the situation is more complicated. The singly occupied states a_{1g} (LUMO) and b_{1g} (HOMO) are mainly formed by one of the—energetically almost degenerate—d_{z^2} and $d_{x^2-y^2}$ orbitals and supported by the s/p orbitals of two axial μ_4-Te atoms (a_{1g}) or four in-plane μ_4-Te atoms (b_{1g}). This means, that a slight tetragonal geometric distortion should prefer one of those states more distinctly.

The charge-partitioning analysis (Table 7) of the $[Co_{11}Te_7(CO)_{10}]^{n-}$ species was performed according to the Hirshfeld scheme.[24] Small positive charges were calculated

Table 7. Charge distribution, according to the Hirshfeld method,[24] of the symmetry-independent atoms within the $[Co_{11}Te_7(CO)_{10}]^{n-}$ series ($n=0-3$) and in $[Co_9Te_6(CO)_8]^{2-}$.

	$[Co_{11}Te_7(CO)_{10}]^{n-}$				$[Co_9Te_6(CO)_8]^{2-}$
	$n=0$	$n=1$	$n=2$	$n=3$	
Co1	−0.1476	−0.1548	−0.1496	−0.1445	−0.1650
Co2	−0.1427	−0.1511	−0.1643	−0.1771	−0.1811
C	0.0889	0.0725	0.0526	0.0321	0.0289
O	−0.0920	−0.1240	−0.1582	−0.1923	−0.1751
Te1	0.2684	0.2020	0.1723	0.1429	0.1683
Te2	0.2135	0.1551	0.1004	0.0459	0.1119

for Te, whereas Co obviously receives the major part of the negative partial charges. Starting from $[Co_{11}Te_7(CO)_{10}]$ and adding the n electrons stepwise, Te1 and Te2 attract most of the additional charge and should therefore take part in charge-transfer processes of the cluster. The contribution of the C atom (carbonyl ligand) remains almost unchanged throughout the series. The O atom of the carbonyl group in $[Co_{11}Te_7(CO)_{10}]^{-}$ takes nearly the same amount and in $[Co_{11}Te_7(CO)_{10}]^{2-}$ it takes even more of the additional charge than Co1. The Co1 charge remains almost constant, whereas that of Co2 decreases slightly. Significant charge separation between Te2 and O is found for the highly charged species $[Co_{11}Te_7(CO)_{10}]^{3-}$, for which the charge compensation limit of the pentagonal prismatic cluster geometry seems to be reached. For $[Co_9Te_6(CO)_8]^{2-}$, the charge-partitioning analysis shows a similar situation. Te2 bears a large amount of charge and the value of Co1 differs significantly from Co2. Oxygen is also very much involved in the charge stabilisation process.

It is of interest in this context, that a low-density surface shows, in the case of $[Co_{11}Te_7(CO)_{10}]^{-}$ (HOMO; Figure 10), a large contact area for reaction partners at the two apical μ_5-Te atoms. Surrounded by CO groups, a "reaction pocket" is formed for Te. This supports the idea that Te could be important for charge transfer. The other information from Figure 10 is the symmetry change between the frontier orbitals of $[Co_{11}Te_7(CO)_{10}]^{-}$ and $[Co_{11}Te_7(CO)_{10}]^{2-}$. A different steric behaviour for interactions with counterions or

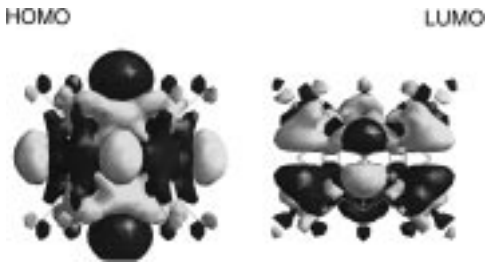

Figure 10. Low-density iso-surface of the HOMO in $[Co_{11}Te_7(CO)_{10}]^{-}$ (left) and $[Co_{11}Te_7(CO)_{10}]^{2-}$ (right) clusters.

reaction partners can be assumed for the latter cluster and no direct pathway of electron-transfer by Te1, for example, is seen here intuitively.

First and second derivatives of the function E versus N (electron number)[25, 26] were calculated to give a quantitative estimation of the chemical potential μ and the chemical hardness η. All the discussed species are relatively soft, that means reactive, in terms of Pearson's definition of chemical hardness. For $[Co_{11}Te_7(CO)_{10}]^{-}$ and $[Co_{11}Te_7(CO)_{10}]^{2-}$, hardness is at a maximum and makes their formation probable. Compared with Co, low-spin valence states of $[Co_2(CO)_8]$, for which Pearson gives the values $\eta = 3.04$ eV and $\mu = 4.12$ eV,[26] $[Co_{11}Te_7(CO)_{10}]^{-}$ ($2\eta = 2.31$ eV, $\mu = 1.77$ eV) and $[Co_{11}Te_7(CO)_{10}]^{2-}$ ($2\eta = 2.29$ eV, $\mu = 1.27$ eV) are found to be less stable. Because of these small values, the discussed compounds should show strong nucleophilic behaviour.

In summary, there is a comparatively high probability for the formation of $[Co_{11}Te_7(CO)_{10}]^{-}$ and $[Co_{11}Te_7(CO)_{10}]^{2-}$. $[Co_{11}Te_7(CO)_{10}]^{-}$ should be the more reactive species, while $[Co_{11}Te_7(CO)_{10}]^{2-}$ has good properties for a stable ground state. For electron-transfer reactions, the low value of the chemical potential of $[Co_{11}Te_7(CO)_{10}]^{2-}$ implies one oxidation step towards the more reactive $[Co_{11}Te_7(CO)_{10}]^{-}$ cluster, which will be formed without a significant loss of bonding energy from $[Co_{11}Te_7(CO)_{10}]^{2-}$. The transformation of $[Co_{11}Te_7(CO)_{10}]^{-}$ into $[Co_{11}Te_7(CO)_{10}]^{2-}$ would occur by occupation of the Co-cage orbitals of the LUMO. The electron density is readily redistributed without large changes in the bond lengths and cluster geometry. Possibly, a small geometric distortion due to Jahn–Teller activity could accompany such a step. Compared with the pentagonal prism $[Co_{11}Te_7(CO)_{10}]^{2-}$, the smaller total energy gain of the cubic cluster $[Co_9Te_6(CO)_8]^{2-}$ makes its formation less probable from a theoretical point of view.

Conclusions

This work focuses on the stepwise formation of metal telluride clusters from molecular units and the investigation of the electron-transfer properties of clusters with a rather unusual pentagonal-prismatic $[Co_{11}Te_7]$ framework. The reactions of $[Cp^{\#}_2NbTe_2H]$ (**1#**) with $[Co_2(CO)_8]$ under varying conditions are mainly characterised by a cross transfer of Te and CO ligands from one metal centre to the other. Only in compounds **2#** are all the building blocks arranged together into a covalent niobocene-cobalttelluride cluster. Addition-

0947-6539/00/0603-0500 $ 17.50+.50/0 *Chem. Eur. J.* **2000**, *6*, No. 3

ally, the formation of the stable salts **4#–6#**, which are composed of discrete ions derived from niobocene and cobalttelluride building blocks, requires charge separations by means of complex electron-transfer reactions.

Complexes **2#** seem to be the first stable intermediates en route to solid-state compounds,[27] but it is striking that $[Co_4(CO)_{10}Te_2]$ (**3**), which simultaneously forms in a good yield (nearly 70%) at 0°C, does not have any "fitting" niobocene counterpart. However, reactive niobocene particles must exist in solution because as the temperature is raised **3** quickly disappears and the cluster salts **5#** and **6#** form. A reaction between **3** and residues of unreacted **1#** can be excluded, since no reaction between **1**(Cp*) and **3** was found in a control experiment in boiling THF. On the other hand, the main structural building blocks of the anions in **5–7** are Co_5Te octahedra, which formally may be derived from Co_4Te_2 octahedra present in **3** by the replacement of a Te vertex by one common Co centre. The role of the hydrogen originally present in **1#** is not yet clear; this is the target of further investigations.

Electrochemical studies provide evidence for four derivatives in the series $[Co_{11}Te_7(CO)_{10}]^{n-}$ ($n=0-3$), thus extending the knowledge about redox-active homoleptic carbonyl transition metal clusters[28] onto the pentagonal prismatic $[Co_{11}Te_7]$ framework. Theoretical calculations support the preferential formation of $[Co_{11}Te_7(CO)_{10}]^-$ and $[Co_{11}Te_7(CO)_{10}]^{2-}$ and provide arguments for the facile transformation $[Co_{11}Te_7(CO)_{10}]^{2-} \rightarrow [Co_{11}Te_7(CO)_{10}]^- + e^-$. It is also shown that the formation of the cubic system $[Co_9Te_6(CO)_8]^{n-}$ ($n=0-2$) is less favourable from an energetic point of view.

Experimental Section

All procedures were carried out under N_2 using dry solvents. Elemental analyses (C, H) were performed at the Mikroanalytisches Laboratorium, Universität Regensburg, or by the Analytische Laboratorien Malissa and Reuter, 51789 Lindlar (Te). IR spectra were obtained with a Beckman 4240 instrument or a Bruker IFS 66v FT IR spectrometer. ^{1}H NMR spectra were recorded with a Bruker WM 250 instrument. Field-desorption mass spectra were obtained on a Finnigan MAT 95 spectrometer. The ESR spectrum was recorded at room temperature on a Bruker ESP 300 spectrometer (field calibration with DPPH ($g=2.0034$). Sephadex LH 20 (Pharmacia Fine Chemicals) was purged with N_2 and then suspended in MeOH saturated with N_2. $[Cp^{\#}_2NbTe_2H]$ (**1#**) was prepared from $[Cp^{\#}_2NbBH_4]$ and Te powder.[5]

Electrochemistry: Cyclic voltammetry was carried out in a standard three-electrode Tacussel UAP 4 unit cell. A saturated calomel electrode (SCE) was used as the reference electrode and was separated from the solution by a sintered glass disk. The auxiliary electrode was a Pt wire. For all voltammetric measurements the working electrode was a carbon or Pt disk electrode, which had been polished with alumina. A three-electrode Tipol polarograph was used for the polarograms. The dropping Hg electrode (DMF) characteristics were $m=3\,mg\,s^{-1}$ and $t=0.5$ s. In all cases, the electrolyte was a 0.2 M solution of nBu_4NPF_6 in THF or CH_2Cl_2. The electrolyses were performed with an Amel 552 potentiostat coupled to an Amel 721 electronic integrator.

DFT calculations: Model calculations for the anionic clusters $[Co_{11}Te_7(CO)_{10}]^{n-}$ ($n=0-3$) and $[Co_9Te_6(CO)_8]^{n-}$ ($n=0$, 2) were performed within the framework of density functional theory (DFT). In an approximation, the coordinates for the atoms, originally taken from the results of the X-ray structure determinations of **5**(Cp*) and **7**(Cp*), were idealised according to complexes with D_{4h} and D_{5h} symmetry, respectively. Assuming that no large changes in the geometry occur during the redox activities of the clusters, single-point calculations were used. Neither counterions nor solvents were included in the model calculations.

The electron density is described in terms of the local density approximation (LDA)[29] and corrected for non-local effects by the application of the Becke–Perdew exchange correlation (BP)[30] to the self-consistent result.[31] A totally symmetric density distribution[32] was used for these model calculations with the DMol program.[33] As basis sets, double-ζ numeric functions extended by one polarisation function were chosen. For purposes of comparison, the mean bonding energies as well as the typical frontier orbitals at low and high densities are determined for the species using different charges. Approximate ionisation potential and chemical hardness of the clusters $[Co_{11}Te_7(CO)_{10}]^{n-}$ were obtained from the slope and the curvature of the function $E_{bonding}$ versus cluster charge. The differences between the atomic energies and the total energies of the clusters, relative to the total number of atoms, are hereby defined as the average bonding energies per atom.

Reaction of $[Cp^{\#}_2NbTe_2H]$ (1#) with $[Co_2(CO)_8]$

At 0°C: A solution of $[Co_2(CO)_8]$ (342 mg, 1.0 mmol) in THF (50 mL) was added dropwise to the ice-cooled solution of **1#** (0.5 mmol) in THF (200 mL). The colour of the solution changed from orange to violet and gas was liberated. After 1 h, the solvent was evaporated at 0°C. The violet residue was dissolved in toluene (10 mL) and CH_2Cl_2 (5 mL). This mixture was then chromatographed on silica gel (column 15 cm, diameter 5 cm) and eluted with toluene to give a violet band which contained **3** in 69% yield. The subsequent green band contained **2#** in strongly varying yields ($\leq$10.7%). Crystals of **2#** were obtained from toluene/pentane 1:2 and crystals of **3** from toluene/pentane 1:1. Complex **2**(Cp*): $C_{27}H_{30}Co_3NbO_7Te_2$ (991.4): calcd C 32.71, H 3.05; found C 33.23, H 3.89.; FD-MS (from toluene): m/z: 989.7 (^{128}Te). Complex **2**(Cp$^{\times}$): $C_{29}H_{34}Co_3NbO_7Te_2$ (1019.5): calcd C 34.17, H 3.36; found C 34.79, H 3.91; FD-MS (from toluene): m/z: 1019.7 (^{128}Te). Complex: **3**: $C_{10}Co_4O_{10}Te_2$ (771.0): calcd C 15.58; found C 15.54.

At 115°C: A mixture of **1#** (0.91 mmol), $[Co_2(CO)_8]$ (615 mg, 1.81 mmol) and toluene (100 mL) was refluxed for 3 h. After vigorous gas evolution a dark powder precipitated, which was separated from the pale yellow liquid phase and washed several times with toluene. All the solutions were combined and the solvent was evaporated. The yellow residue was dissolved in MeOH (15 mL). Filtration on Sephadex LH 20 gave 100 mg (19%, Cp*) and 35 mg (6.2%, Cp$^{\times}$) of yellow **4#**. The compounds were recrystallised from CH_2Cl_2/pentane 5:1. Recrystallisation of the dark residue from hot acetonitrile (50–60 mL) gave, after cooling to ambient temperature, dark brown prisms and needles consisting of **5#** and **6#**. Crystallisation was completed by cooling to −25°C (total yield 420 mg). All yields are based on **1#**. Complexes **5**(Cp*) and **6**(Cp*) were identified and characterised by manual separation under the microscope and X-ray structure determination. For analytical purposes the crystalline material was analysed together, the results are given in Table 8. Complex **4**(Cp*): $C_{26}H_{30}CoNbO_6$ (590.5): calcd C 52.90, H 5.12; found C 52.61, H 5.21; FD-MS (from acetone): m/z 419.4 $[Cp^*_2Nb(CO)_2]^+$. Complex **4**(Cp$^{\times}$): $C_{28}H_{34}CoNbO_6$ (618.4): calcd C 54.38, H 5.54; found C 53.96, H 5.44; FD-MS (from acetone): m/z 447.4 $[Cp^{\times}_2Nb(CO)_2]^+$.

Preparation of $[Cp^{\#}_2Nb(CO)_2][Co_{11}Te_7(CO)_{10}]$ (7#)

Method A: The residues which had been washed with toluene in the reaction described above were dried in vacuo and then dissolved in CH_2Cl_2 (12 mL). Chromatography on silica gel (column length 10 cm, diameter 3 cm) gave a dark red-brown band upon elution with CH_2Cl_2 which contained **7**(Cp*) (420 mg, 0.187 mmol, 42% based on **1**(Cp*)) and **7**(Cp$^{\times}$) (650 mg, 0.286 mmol, 64% based on **1**(Cp$^{\times}$)). Recrystallisation of **7#** from CH_2Cl_2 gave dark brown needles (Table 8).

Method B: A mixture of **5**(Cp*)/**6**(Cp*) (112 mg), CH_2Cl_2 (50 mL), and HPF_6 (9.5 mg, 0.065 mmol, 65% in H_2O) was stirred for 2 h at room temperature. After evaporation of the solvent, the dark brown residue was washed with H_2O (2 × 30 mL) to give 85 mg of **7**(Cp*). The vacuum-dried powder gave the correct analyses (Table 8).

Crystal structure determination for 2(Cp$^{\times}$), 4(Cp$^{\times}$), 5(Cp*), and 7(Cp*):[34] Crystal data and details of the measurements are summarised in Table 9. The structures were solved by direct methods and least-squares refinement. Program packages SHELXTL PLUS (Release 4.2/800) were employed for

Table 8. Elemental analyses of complexes **5**–**7**.

		M.W.	C (calcd)	H (calcd)	C (found)	H (found)	remarks
5(Cp*)	$C_{52}H_{60}Co_9Nb_2O_{12}Te_6$	2358.85	26.48	2.56			[a]
6(Cp*)	$C_{54}H_{60}Co_{11}Nb_2O_{14}Te_7$	2660.34	24.38	2.27			[a]
5(Cp$^\times$)	$C_{56}H_{68}Co_9Nb_2O_{12}Te_6$	2414.96	27.85	2.84	25.24	2.93	
6(Cp$^\times$)	$C_{58}H_{68}Co_{11}Nb_2O_{14}Te_7$	2716.45	25.65	2.52	25.24	2.93	
7(Cp*)	$C_{32}H_{30}Co_{11}NbO_{12}Te_7$	2240.95	17.15	1.35	17.28	1.56	Method A[b]
					17.15	1.98	Method B
7(Cp$^\times$)	$C_{34}H_{34}Co_{11}NbO_{12}Te_7$	2269.01	18.00	1.51	18.43	2.15	

[a] C values have been found between 24.05 and 25.91 % for the mixture **5**(Cp*)/**6**(Cp*). [b] Te (calcd) 39.37, Te (found) 39.86.

Table 9. X-ray crystallographic data for complexes **2**(Cp$^\times$), **4**(Cp$^\times$), **5**(Cp*) and **7**(Cp*).

	2(Cp$^\times$)	**4**(Cp$^\times$)	**5**(Cp*)	**7**(Cp*)
formula	$C_{29}H_{34}Co_3NbO_7Te_2$	$C_{28}H_{34}CoNbO_6$	$C_{52}H_{60}Co_9Nb_2O_{12}Te_6$	$C_{32}H_{30}Co_{11}NbO_{12}Te_7$
M_W	1020.0	618.4	2358.9	2240.9
T [°C]	20	20	25	20
crystal size [mm]	0.25 × 0.65 × 0.65	0.10 × 0.45 × 0.90	0.20 × 0.09 × 0.04	0.05 × 0.10 × 0.40
crystal system	monoclinic	triclinic	monoclinic	monoclinic
space group	$P2_1/n$ (No. 14)	$P\bar{1}$ (No. 2)	$C2/c$ (No. 15)	$P2_1/m$ (No. 11)
a [Å]	9.069(5)	9.727(2)	16.331(2)	11.639(3)
b [Å]	19.74(1)	11.375(2)	25.323(2)	16.297(3)
c [Å]	19.34(1)	13.247(2)	16.767(2)	13.537(3)
α [°]		98.72(3)		
β [°]	94.96(5)	92.62(3)	106.55(1)	96.74(2)
γ [°]		94.30(3)		
V [Å^3]	3449(4)	1442.2(6)	6646.7(8)	2550(1)
Z	4	2	4	2
ρ_{calcd} [g cm^{-3}]	1.96	1.42	2.365	2.92
μ [$Mo_{K\alpha}$, mm^{-1}]	3.44	1.01	5.15	7.67
instrument	syntex R3	syntex R3	Stoe-IPDS	syntex R3
scan range	$3.0 < 2\theta < 52.5$	$3.0 < 2\theta < 57.5$	$2.05 < Q < 25.54$	$3.0 < 2\theta < 57.0$
reflns collected	7646	7496	15383	6986
unique	6986		6129	6685
observed [$I > 2.5\sigma(I)$]	4377	4695	3005[a]	3255
parameters	382	326	368	307
transmission	0.44 – 1.00	0.86 – 1.00	0.449 – 0.586	0.88 – 1.00
max/min residual density [e Å^{-3}]	1.63/ – 0.72	0.91/ – 0.91	0.618/ – 0.452	1.37/ – 1.60
$R1$	0.060	0.064	0.026	0.061
$wR2$	0.048	0.053	0.038	0.048

[a] $I > 2.0\sigma(I)$.

2(Cp$^\times$), **4**(Cp$^\times$) and **7**(Cp*), and SIR-97, SHELXL97 for **5**(Cp*) with all unique reflections. Non-hydrogen atoms were refined anisotropically, and hydrogen atoms were added in calculated positions. In **2**(Cp$^\times$) a 94:6 disorder was found for the Co_3 plane.

Acknowledgements

We thank Prof. Dr. G. Huttner for his help with the X-ray crystallography and Prof. Dr. K.-J. Range for his constant support. We are also grateful to Mr. Walter Meier for technical assistance. We gratefully acknowledge financial support from the Deutsche Forschungsgemeinschaft (Grant Wa 485/6-1).

[1] J. W. Kolis, *Coord. Chem. Rev.* **1990**, *105*, 195; L. C. Roof, J. W. Kolis, *Chem. Rev.* **1993**, *93,* 1037.

[2] W. S. Sheldrick, M. Wachhold, *Angew. Chem.* **1995**, *107*, 490; *Angew. Chem. Int. Ed. Engl.* **1995**, *34*, 450; M. G. Kanatzidis, *Angew. Chem.* **1995**, *107*, 2281; *Angew. Chem. Int. Ed. Engl.* **1995**, *34*, 2109; Q. Liu, N. Goldberg, R. Hoffmann, *Chem. Eur. J.* **1996**, *2*, 390; Y. V. Mironov, M. A. Pell, J. A. Ibers, *Angew. Chem.* **1996**, *108*, 2999; *Angew. Chem. Int. Ed. Engl.* **1996**, *35*, 2854.

[3] J. F. Corrigan, D. Fenske, *Chem. Commun*. **1996**, 943; J. F. Corrigan, D. Fenske, W. P. Power, *Angew. Chem*. **1997**, *109*, 1224; *Angew. Chem. Int. Ed. Engl.* **1997**, *36*, 1176; J. F. Corrigan, D. Fenske, *Angew. Chem*. **1997**, *109*, 2070; *Angew. Chem. Int. Ed. Engl.* **1997**, *36*, 1981; J. F. Corrigan, D. Fenske, *Chem. Commun*. **1997**, 1836.

[4] M. L. Steigerwald, T. Siegrist, S. M. Stuczynski, *Inorg. Chem*. **1991**, *30*, 4940.

[5] O. Blacque, H. Brunner, M. M. Kubicki, B. Nuber, B. Stubenhofer, J. Wachter, B. Wrackmeyer, *Angew. Chem*. **1997**, *109*, 361; *Angew. Chem*. *Int. Ed. Engl.* **1997**, *36*, 351.

[6] M. M. Kubicki, P. Oudet, C. Martin, C. Barré, *J. Chem. Soc. Dalton Trans*. **1995**, 3699.

[7] N. I. Kirillova, A. I. Gusev, A. A. Pasynskii, Y. T. Struchkov, *Zh. Strukt. Khim*. **1974**, *14*, 812.

[8] R. C. Ryan, L. F. Dahl, *J. Am. Chem. Soc*. **1975**, *97*, 6904.

[9] For references see: R. M. DeSilva, M. J. Mays, J. E. Davies, P. R. Raithby, M. A. Rennie, G. P. Shield, *J. Chem. Soc. Dalton Trans.* **1998**, 439.

[10] D. Braga, F. Grepioni, G. R. Desiraju, *J. Organomet. Chem.* **1997**, *548*, 33.

[11] H. Brunner, G. Gehart, W. Meier, J. Wachter, A. Riedel, S. Elkrami, Y. Mugnier, B. Nuber, *Organometallics* **1994**, *13*, 134.

[12] D. J. Sikora, M. D. Rausch, R. D. Rogers, J. L. Atwood, *J. Am. Chem. Soc*. **1981**, *103*, 1265.

[13] F. Calderazzo, I. Ferri, G. Pampaloni, U. Englert, *Organometallics* **1999**, *18*, 2452.

  0947-6539/00/0603-0502 $ 17.50+.50/0 *Chem. Eur. J.* **2000**, *6*, No. 3

[14] J. G. Brennan, T. Siegrist, S. M. Stuczinski, M. L. Steigerwald, *J. Am. Chem. Soc.* **1989**, *111*, 9240.
[15] G. Christou, K. S. Hagen, J. K. Bashkin, R. H. Holm, *Inorg. Chem.* **1985**, *24*, 1010.
[16] D. Fenske, J. Ohmer, K. Merzweiler, *Angew. Chem.* **1988**, *100*, 1572; *Angew. Chem. Int. Ed. Engl.* **1988**, *27*, 1512; D. Fenske, H. Fleischer, C. Persau, *Angew. Chem.* **1989**, *101*, 1740; *Angew. Chem. Int. Ed. Engl.* **1989**, *28*, 1665; D. Fenske, C. Persau, *Z. Anorg. Allg. Chem.* **1991**, *593*, 61; J. P. Zebrowski, R. K. Hayaski, A. Bjarnason, L. F. Dahl, *J. Am. Chem. Soc.* **1992**, *114*, 3121.
[17] E. Furet, A. Le Beuze, J.-F. Halet, J.-Y. Saillard, *J. Am. Chem. Soc.* **1995**, *117*, 4936.
[18] B. Zouchoune, F. Ogliaro, J.-F. Halet, J.-Y. Saillard, J. R. Eveland, K. H. Whitmire, *Inorg. Chem.* **1998**, *37*, 865.
[19] R. Seidel, R. Kliss, S. Weissgräber, G. Henkel, *J. Chem. Soc. Chem. Commun*. **1994**, 2791.
[20] H. Brunner, J.-C. Leblanc, D. Lucas, W. Meier, C. Moise, Y. Mugnier, B. Nuber, S. Rigny, A. Sadorge, J. Wachter, *J. Organomet. Chem.* **1998**, *566*, 203.
[21] Y. Mugnier, P. Reeb, C. Moise, E. Laviron, *J. Organomet. Chem.* **1983**, *254*, 111; P. Reeb, Y. Mugnier, C. Moise, E. Laviron, *J. Organomet. Chem.* **1984**, *273*, 247.
[22] E. Furet, A. Le Beuze, J.-F. Halet, J.-Y. Saillard, *J. Am. Chem. Soc.* **1994**, *116*, 274.
[23] S. Nomiko, B. Schubert, R. Hoffmann, M. L. Steigerwald, *Inorg. Chem.* **1992**, *31*, 2201.
[24] F. L. Hirshfeld, *Theor. Chim. Acta*, **1977**, *44*, 129.
[25] R. G. Parr, W. Yang, *Density Functional Theory of Atoms and Molecules,* Oxford University Press, **1989**.
[26] R. G. Pearson, *Chemical Hardness*, Wiley-VCH, **1996**.
[27] M. L. Steigerwald, T. Siegrist, S. M. Stuczynski, *Inorg. Chem*. **1991**, *30*, 2256.
[28] F. Calderoni, F. Demartin, F. F. de Biani, C. Femoni, M. C. Iapalucci, G. Longoni, P. Zanello, *Eur. J. Inorg. Chem.* **1999**, 663, and references cited therein.
[29] W. Kohn, *Phys. Rev. A* **1986**, *34*, 737.
[30] A. D. Becke, *Phys. Rev. A* **1988**, *38*, 3098; J. P. Perdew, *Phys. Rev. B* **1986**, *33*, 8822.
[31] M. J. Lidell, *J. Organomet. Chem.* **1998**, *565*, 271.
[32] C. Jamorski, A. Martinez, M. Castro, D. Salahub, *Phys. Rev. B* **1997**, *55*, 10905.
[33] Program Package DMOL, *Cerius*^{2} *User Guide* **1997**, Molecular Simulations, San Diego.
[34] Crystallographic data (excluding structure factors) for the structures reported in this paper have been deposited with the Cambridge Crystallographic Data Centre as supplementary publication no. CCDC-127033 **2**(Cp$^\times$), 127034 **4**(Cp$^\times$), 127035 **5**(Cp*), and 127036 **7**(Cp*). Copies of the data can be obtained free of charge on application to CCDC, 12 Union Road, Cambridge CB2 1EZ, UK (Fax: (+44) 1223-336-033; e-mail: deposit@ccdc.cam.ac.uk).

Received: July 9, 1999 [F1896]